On the overall yielding of an isotropic porous material with a matrix obeying a non-quadratic criterion

Stefan C. Soare[a]

[a]Technical Univ. of Cluj-Napoca, 28 Memorandumului, 400114 Cluj-Napoca, Romania

(October 30, 2015)

Abstract

A general methodology is outlined for the investigation and modeling of the overall yield function of a representative volume element (RVE) of a porous metal. Illustrations are shown for an idealized RVE in the form of a hollow sphere with von Mises and Hershey-Hosford matrix, respectively. In both cases the yield surface is revealed to have a complex geometry, the most notable feature being the asymmetry with respect to the origin of the stress space in the range of high triaxialities.

Keywords: Plasticity, Ductile damage, Yield function, Homogenization

1. Introduction

Modeling the plastic deformation of metals while taking into account the gradual deterioration of their load carrying capacity due to the nucleation, growth and coalescence of voids (or pores) at microstructural level has been and still is an active field of research, motivated by important practical applications.

By contrast with the "classical" incompressible plastic behavior[1], a distinctive characteristic of porous metals, manifesting at the macroscopic level of observation, is that they feature a significant volumetric component of plastic deformation, or, equivalently, that their stress-strain response is influenced by the hydrostatic component of the stress state. This is explained by the fact that, even if the macroscopically applied stress is purely hydrostatic, the stress field generated at microscopic level has in general a non-vanishing deviatoric component, being thus capable of plastically deforming a plastically incompressible matrix (sound material).

The first isotropic yield function inspired by the just described micro-mechanism was proposed by Gurson (1977) in the form

$$\mathcal{F}(\boldsymbol{\Sigma}, f, \bar{\epsilon}_p) = \frac{\Sigma_{eq}^2}{H^2} + 2f\cosh\left(\frac{3\Sigma_m}{2H}\right) - 1 - f^2 \tag{1}$$

where $\boldsymbol{\Sigma}$ denotes the macroscopic (or, from an averaging perspective, the overall) Cauchy stress, $\Sigma_m := \mathrm{tr}\boldsymbol{\Sigma}$ its hydrostatic component, $\boldsymbol{\Sigma'} := \boldsymbol{\Sigma} - \Sigma_m \boldsymbol{I}$ its deviatoric part, and $\Sigma_{eq} := \sqrt{3/2}|\boldsymbol{\Sigma'}|$ its von Mises norm; the parameter $\bar{\epsilon}_p$ represents a macroscopic equivalent plastic strain, with $H = H(\bar{\epsilon}_p)$ representing isotropic hardening, while f is a measure of the porosity of the material.

The expression in eq.(1) was deduced by Gurson based on the analysis of the rigid-plastic response of a representative volume element (RVE) idealized in the form of a hollow sphere. However, put in a wider perspective, formula (1) appears to be a fortunate event: Indeed, further extensions of Gurson's analysis, amenable to explicit calculations, seem possible only when the matrix is governed by a quadratic yielding criterion, von Mises or Hill'48, e.g., Liao et al (1997), Benzerga and Besson (2001). While adequate for certain steels, this description of matrix yielding is less suited, for example, in the case of non-ferrous metals such as aluminum or magnesium alloys. Then a more realistic modeling of the progress of damage by void growth, in a wider range of materials, requires the consideration of more general descriptions of matrix yielding behavior.

In this context, by comparison with the von Mises function, the Hershey (1954) and Hosford (1972) function[2]

$$g(\boldsymbol{\sigma}) = k_n\left[(\sigma_1 - \sigma_2)^n + (\sigma_2 - \sigma_3)^n + (\sigma_3 - \sigma_1)^n\right]^{1/n} \tag{2}$$

with exponents $n = 6$ or 8, is known to be closer to the experimental data of many materials with face centred cubic lattice, particularly aluminum. The main objective here is to obtain an estimate of the overall yield function of an RVE idealized as a hollow sphere whose matrix is rigid, perfectly plastic and governed by the Hershey-Hosford yield function. As methodology, we shall adopt the same framework as in Gurson (1977) or Leblond (2003), but, instead of pursuing explicit calculations, we look for best approximations in an appropriate set of functions.

At this point it must be mentioned that other approaches, some extending the Hashin-Shtrikman variational lemma for elastic bodies to nonlinear stress-strain relationships in potential form, e.g., Castaneda (1991), Willis (1991), while others adopting right from the outset an interpolative approach, e.g., Cocks (1989), Michel and Suquet (1992), describe the overall response of a porous material using a homogeneous yield function of the form

$$\mathcal{F}(\boldsymbol{\Sigma}, f, \bar{e}_p) = \left[A(f)\Sigma_{eq}^2 + B(f)\Sigma_m^2\right]^{1/2} - H(\bar{e}_p) \tag{3}$$

The parameters A and B are specific to each approach, but it may already be noted that they can be linked to purely deviatoric and hydrostatic responses at macro-level, respectively. In general, the above quadratic provides a satisfactory description only for large porosity ratios, e.g., $f \geq 0.01$, its performance being quite poor for lower porosities, the case most

[1]Where the volumetric component of deformation is elastic and hence negligible.

[2]σ_i are the principal values of the stress state $\boldsymbol{\sigma}$ and $k_n = 2^{-1/n}$ is a normalization constant chosen such that the yielding criterion $g(\boldsymbol{\sigma}) = h$ reduces to $\tau = h$ for uniaxial stress states of magnitude τ.

often encountered in practice. This suggests that higher order polynomial combinations should be used for an improved description.

Then the course of this investigation is as follow. First, the general homogenization framework together with some preliminary remarks are presented in section 2; in section 3.1 is described a numerical approach for the investigation of the overall yield surface of an RVE with matrix governed by an arbitrary yield function; applications to the cases $n = 2$ and $n = 8$ in eq.(2) are featured in sections 3.2 and 3.3, respectively; finally, conclusions are drawn in section 4.

2. Constitutive framework, averaging considerations and preliminary remarks

The object of study here is a representative volume element (RVE) of a macroscopic body of material whose overall response is to define the constitutive response of a particle X of a continuum model of the body. The RVE occupies a domain Ω, with a subset $\omega \subset \Omega$ occupied by voids, the sound material, or matrix, occupying the set $\Omega \setminus \omega$. The porosity of the RVE is then the fraction $f := |\omega|/|\Omega|$.

We seek the response of the RVE when the macroscopic rate of deformation $\boldsymbol{D}$ at particle X is prescribed. Then the fundamental homogenization assumption is

$$\boldsymbol{v}(x,t) = \boldsymbol{D}(t) : x, \quad x \in \partial\Omega \tag{4}$$

where x denotes positions of particles of the RVE with respect to some laboratory frame, $\boldsymbol{v}$ is the velocity field within the RVE and $\partial\Omega$ is the (outer) boundary of the set Ω.

Any velocity field satisfying the boundary condition (4) is called *admissible*. The corresponding field of rate of deformation $\boldsymbol{d} = (1/2)[\partial\boldsymbol{v}/\partial x + (\partial\boldsymbol{v}/\partial x)^T]$ determines the stress field within the RVE via the constitutive law, which here, for a rigid, perfectly plastic matrix, is in the form of the system

$$\sigma_{eq} - h = 0, \quad \text{with } \sigma_{eq} := g(\boldsymbol{\sigma}) \tag{5}$$

$$\boldsymbol{d} = \dot{\lambda}\frac{\partial g}{\partial \boldsymbol{\sigma}}(\boldsymbol{\sigma}) \tag{6}$$

where the first equation states the yielding condition and the second, the (associated) flow rule. The function g is assumed to be pressure-independent, positive *homogeneous* and *convex*, thus defining a norm on the subspace of deviatoric stresses usually denoted σ_{eq} and referred to as *equivalent stress*. Convexity then implies that the above system has a unique solution[3] $\boldsymbol{\sigma} = \boldsymbol{\sigma}(\boldsymbol{d})$.

In this way, with each function g, or with each convex set, one associates a dissipation function

$$\pi(\boldsymbol{d}) := \boldsymbol{\sigma} \cdot \boldsymbol{d} = h\dot{\lambda} \tag{7}$$

where for each $\boldsymbol{d}$, $\boldsymbol{\sigma}(\boldsymbol{d})$ is the unique solution of the system (5-6), the second equality following from the homogeneity of g. Note that since $\boldsymbol{\sigma}(\alpha\boldsymbol{d}) = \boldsymbol{\sigma}(\boldsymbol{d})$, for any $\alpha > 0$, π is a positive *homogeneous* function. Conversely, given a first degree positive homogeneous function $\pi = \pi(\boldsymbol{d})$, one defines in the space of stress tensors the set

$$C_\pi := \{\boldsymbol{\sigma} \,|\, \boldsymbol{\sigma} \cdot \boldsymbol{d} \leq \pi(\boldsymbol{d}),\ (\forall)\boldsymbol{d}\} \tag{8}$$

which is convex (as an intersection of half-spaces). To each $\boldsymbol{d}$ there corresponds a unique $\boldsymbol{\sigma} \in \partial C_\pi$, the point where a hyperplane orthogonal to $\boldsymbol{d}$ is tangent at the boundary of C_π. Thus ∂C_π admits a parametrization $\boldsymbol{\sigma} = \boldsymbol{\sigma}(\boldsymbol{d})$. This is related to the dissipation function by noting that on ∂C_π there holds $\boldsymbol{\sigma} \cdot \boldsymbol{d} = \pi(\boldsymbol{d})$; differentiating with respect to d_{ij} obtains the identity

$$\frac{\partial \boldsymbol{\sigma}}{\partial d_{ij}} \cdot \boldsymbol{d} + \boldsymbol{\sigma} = \frac{\partial \pi}{\partial d_{ij}}$$

Given a pair $\boldsymbol{d}^*$ and its corresponding $\boldsymbol{\sigma}^*$, in the space of rate of deformations we may consider a curve $\boldsymbol{d} = \boldsymbol{d}(\tau)$, with τ a numerical parameter, such that $\boldsymbol{d}(\tau^*) = \boldsymbol{d}^*$ and having an arbitrarily prescribed tangent $(d/d\tau)\boldsymbol{d}(\tau^*) =: \dot{\boldsymbol{d}}$. Then $\boldsymbol{\sigma}(\tau) = \boldsymbol{\sigma}(\boldsymbol{d}(\tau))$ is a curve on ∂C_π passing through $\boldsymbol{\sigma}^*$ with the tangent $\boldsymbol{v} = \partial\boldsymbol{\sigma}/\partial\boldsymbol{d} : \dot{\boldsymbol{d}}$; since $\boldsymbol{v}$ is in the tangent hyperplane at $\boldsymbol{\sigma}^*$, there holds $\boldsymbol{d} \cdot (\partial\boldsymbol{\sigma}/\partial\boldsymbol{d} : \dot{\boldsymbol{d}}) = 0$, for arbitrary $\dot{\boldsymbol{d}}$. Thus $(\partial\boldsymbol{\sigma}/\partial\boldsymbol{d})(\boldsymbol{\sigma}^*) : \boldsymbol{d}^* = \boldsymbol{0}$ and the above identity results into the sought parametrization of ∂C_π:

$$\boldsymbol{\sigma}(\boldsymbol{d}) = \frac{\partial \pi}{\partial \boldsymbol{d}}(\boldsymbol{d}) \tag{9}$$

Let us also recall that the convexity of C_π is equivalent to the following inequality, commonly referred to as the principle of maximum dissipation: given $\boldsymbol{d}$ and its corresponding $\boldsymbol{\sigma}(\boldsymbol{d}) \in \partial C_\pi$, for any $\boldsymbol{\sigma}^* \in C_\pi$ there holds $(\boldsymbol{\sigma}^* - \boldsymbol{\sigma}) \cdot \boldsymbol{d} \leq 0$. With the indicator function δ_A of a set A defined by

$$\delta_A(p) = \begin{cases} 0, & \text{if } p \in A \\ +\infty, & \text{if } p \notin A \end{cases}$$

this implies that the dissipation function of the convex C_π admits the representation

$$\pi(\boldsymbol{d}) = \sup_{\boldsymbol{\sigma}^* \in C_\pi} \boldsymbol{\sigma}^* \cdot \boldsymbol{d} = \delta^*_{C_\pi}(\boldsymbol{d}) \tag{10}$$

[3]Geometrically, this is obvious: for any "vector" $\boldsymbol{d}$ issued at the origin of the stress space, there exists a unique point $\boldsymbol{\sigma}$ of the surface defined by eq.(5) such that $\boldsymbol{d}$ is along the exterior normal to the surface at $\boldsymbol{\sigma}$.

where, given a numerical function $\phi = \phi(p)$ over a vector space V, its Legendre-Fenchel transform ϕ^* is defined over the same space V by $\phi^*(q) = \sup\{q \cdot p - \phi(p) \,|\, p \in V\}$. Since δ_{C_π} is a convex function, there holds

$$\pi^*(\boldsymbol{\sigma}) = \delta^{**}_{C_\pi}(\boldsymbol{\sigma}) = \delta_{C_\pi}(\boldsymbol{\sigma}) \tag{11}$$

The same construction can be repeated at macro-level, in terms of analogues constitutive macro-objects, to describe the overall response of the RVE. By definition, for any stress distribution $\boldsymbol{\sigma}$ within the RVE, its corresponding macro-stress $\boldsymbol{\Sigma}$ is

$$\boldsymbol{\Sigma} := \frac{1}{|\Omega|} \int_{\Omega\setminus\omega} \boldsymbol{\sigma}\, dx \tag{12}$$

The *actual* velocity field $\boldsymbol{v}$ within the RVE is determined by a boundary value problem consisting of the equilibrium equation, $\mathrm{div}(\boldsymbol{\sigma}) = \mathbf{0}$, the constitutive system (5-6) or the representation (9), and the boundary condition (4). This in turn determines the fields $\boldsymbol{d}$ and $\boldsymbol{\sigma}$ as functions of the macro-rate of deformation $\boldsymbol{D}$. In particular, the macro-stress itself is a function $\boldsymbol{\Sigma} = \boldsymbol{\Sigma}(\boldsymbol{D})$ and hence an overall dissipation function can be defined for the RVE by

$$\Pi(\boldsymbol{D}) := \boldsymbol{\Sigma} \cdot \boldsymbol{D} = \frac{1}{|\Omega|} \int_{\Omega\setminus\omega} \pi(\boldsymbol{d})\, dx \tag{13}$$

the second equality resulting from Hill's Lemma (applied to the fields $\boldsymbol{\sigma}$ and $\boldsymbol{d}$, equilibrated and compatible, respectively). Similar to eqs.(8) and (9), the macro-dissipation (13) defines the macroscopic rigidity (or elasticity) domain

$$C_\Pi := \{\boldsymbol{\Sigma} \,|\, \boldsymbol{\Sigma} \cdot \boldsymbol{D} \le \Pi(\boldsymbol{D}),\ (\forall)\boldsymbol{D}\} \tag{14}$$

which is parameterized by

$$\boldsymbol{\Sigma}(\boldsymbol{D}) = \frac{\partial \Pi}{\partial \boldsymbol{D}}(\boldsymbol{D}) \tag{15}$$

Alternatively, C_Π, being a convex set, admits a description in the form

$$\mathcal{F} := \mathcal{G}(\boldsymbol{\Sigma}, f) - H \le 0 \tag{16}$$

where $\mathcal{G}$ is a first degree positive homogeneous function and H a macroscopic measure of hardening. Since here we are concerned only with the description of the *isotropic* approximation of the macroscopic response, the only parameter reflecting the "void" microstructure is its porosity f.

With the flow rule (in the form of the normality rule) resulting from the characterization in eq.(14), the yield function $\mathcal{F}$ is the central constitutive element of the overall response of the RVE. In theory, it could be found by first calculating the macro-dissipation Π, then the (explicit) parametrization in eq.(15) in terms of D_{ij}, and finally the corresponding implicit form (after eliminating the parameters D_{ij}). In practice, it is difficult to follow this program for two main reasons: (**i**) even for simple, highly idealized RVE's, obtaining the exact velocity field within the RVE is possible only in few particular cases, usually when the boundary condition (4) complies with some of the symmetries of the RVE; (**ii**) explicit quadratures of the integrals involved are rarely possible.

The difficulties mentioned at (**i**) are usually circumvented by replacing the actual velocity field with a reasonable approximation, with the requirement that the latter be admissible (that is, it satisfies eq.(4)). This leads to an upper bound estimate of the macro dissipation: for $\boldsymbol{v}$ and $\boldsymbol{v}^*$, the actual and an arbitrary admissible velocity field, respectively, by eq.(13) there holds

$$\begin{aligned} |\Omega|\Pi(\boldsymbol{D}) = \int_{\Omega\setminus\omega} \boldsymbol{\sigma}\cdot\boldsymbol{d}\, dx = \int_{\partial\Omega} \sigma_{ip} v_i n_p\, da = \\ \int_{\partial\Omega} \sigma_{ip} v^*_i n_p\, da = \int_{\Omega\setminus\omega} \boldsymbol{\sigma}\cdot\boldsymbol{d}^* dx \le \int_{\Omega\setminus\omega} \boldsymbol{\sigma}^*\cdot\boldsymbol{d}^* dx \end{aligned} \tag{17}$$

where the second equality holds because $\partial\omega$ is traction-free, and the last inequality holds by virtue of the maximum dissipation inequality. The last term in the above sequence defines a dissipation function $\Pi^+(\boldsymbol{D}) \ge \Pi(\boldsymbol{D})$. Our main objective is to obtain accurate approximations of the upper bound $\Pi^+(\boldsymbol{D})$ corresponding to a given approximation of the velocity field.

Here we consider an RVE occupying a ball of radius b, with the sound material filling the set $a \le r \le b$, where $a > 0$ and $b > a$ are the inner and outer radii of the RVE, and $r := |x|$ is the distance from the origin of the (orthogonal) coordinate system, at the center of the RVE, to the particle at x. The corresponding spherical coordinates of the particle are $r > 0$, $\phi \in [0, \pi)$ and $\theta \in [0, 2\pi]$, with the local frame denoted $\{\boldsymbol{e}_r, \boldsymbol{e}_\theta, \boldsymbol{e}_\phi\}$.

The velocity field within the RVE will be approximated by

$$\boldsymbol{v}(x) = \boldsymbol{D'} : x + \frac{b^3 D_m}{r^3}\, x \tag{18}$$

This formula, a particular case of a representation used by Rice and Tracey (1969) for an unbounded RVE, was employed by Gurson in his analysis of a finite spherical RVE, and has since become the starting point for many generalizations. Despite it not being an accurate estimate for arbitrary boundary conditions, three features have consecrated it: 1) the field is admissible;

2) it is exact when $\boldsymbol{D} = D_m \boldsymbol{I}$, that is, for purely spherical loading; 3) it is simple enough to allow, at least in the case of a "quadratic" matrix, for some explicit calculations, e.g., Gurson (1977), Liao et al (1997), Benzerga and Besson (2001).

The field of rate of deformation corresponding to (18) is:

$$\boldsymbol{d}(x) = \boldsymbol{D'} + \frac{b^3 D_m}{r^3}\left(\boldsymbol{I} - 3\boldsymbol{e}_r \otimes \boldsymbol{e}_r\right) \tag{19}$$

As preliminary remarks, regarding the overall yield function $\mathcal{F}$ of the RVE, we can already observe some of its analytical features, following from eq.(19).

First, independently of eq.(19), a direct application of Jensen's inequality for convex functions, in integral form, obtains:

$$g\left(\int_{\Omega\setminus\omega} \boldsymbol{\sigma} dx\right) \leq \int_{\Omega\setminus\omega} g(\boldsymbol{\sigma}) dx \leq (|\Omega| - |\omega|)h$$

where in the second inequality we used the fact that $g(\boldsymbol{\sigma}) \leq h$, at all points $x \in \Omega \setminus \omega$, and that h is constant (in time), thus uniform over $\Omega \setminus \omega$. Dividing by $|\Omega|$, using the homogeneity of g and its pressure-independence, recalling the definition of the macro-stress (12) and that of the porosity f, result in the relationship

$$g(\boldsymbol{\Sigma'}) \leq (1-f)h \tag{20}$$

Thus the macro rigidity (elastic) domain C_Π is always contained within the cylinder defined by the above inequality[4]. This is a universal bound, holding for any measure g of equivalent stress. In particular, in the case of the von Mises matrix, inspection of eq.(1) shows that Gurson's function does not improve upon this bound when restricted to the subspace of deviatoric stress states. This is no accident, for it can be shown that eq.(18), or (19), leads precisely to the bound in eq.(20), on the subspace of deviatoric stresses.

Indeed, when $D_m = 0$, and recalling the representation in eq.(10), eqs.(13) and (19) imply

$$\delta^*_{C_\Pi}(\boldsymbol{D'}) = \Pi(\boldsymbol{D'}) = (1-f)\pi(\boldsymbol{D'}) = (1-f)\delta^*_{C_\pi}(\boldsymbol{D'}) \tag{21}$$

But for any set K and any $\lambda > 0$ there holds $\delta^*_{\lambda K} = \lambda \delta^*_K$; also, letting K' denote the projection of the set K on the subspace of deviatoric stresses, $\delta^*_K(\boldsymbol{D'}) = \delta^*_{K'}(\boldsymbol{D'})$. Then eq.(21) rewrites:

$$\delta^*_{C'_\Pi}(\boldsymbol{D'}) = \delta^*_{(1-f)C'_\pi}(\boldsymbol{D'})$$

for any deviatoric macro-rate of deformation $\boldsymbol{D'}$. Then recalling eq.(11), taking the conjugate, with respect to the subspace of deviatoric stresses, of each member of this equality obtains

$$\delta_{C'_\Pi}(\boldsymbol{\Sigma'}) = \delta_{(1-f)C'_\pi}(\boldsymbol{\Sigma'}), \forall \boldsymbol{\Sigma'} \iff C'_\Pi = (1-f)C'_\pi$$

Thus, when restricted to the subspace of deviatoric macro-stresses, the overall yield function resulting from the velocity field (18) is identical with the relationship in eq.(20). In the context of eq.(16), and defining the macro-measure of hardening by $H := h$, this means that

$$\mathcal{G}(\boldsymbol{\Sigma'}, f) = \frac{1}{1-f}\, g(\boldsymbol{\Sigma'}) \tag{22}$$

The other case where an exact formula can be deduced is when $\boldsymbol{D'} = \boldsymbol{0}$, that is, in the spherically symmetric case when $\boldsymbol{D} = D_m \boldsymbol{I}$. Here, due to isotropy, the stress field within the RVE also is spherically symmetric, at each particle having the form $\boldsymbol{\sigma} = \sigma_r \boldsymbol{e}_r \otimes \boldsymbol{e}_r + \sigma_\theta(\boldsymbol{e}_\theta \otimes \boldsymbol{e}_\theta + \boldsymbol{e}_\phi \otimes \boldsymbol{e}_\phi)$. Assuming that the whole matrix has yielded, there holds $g(\sigma_r, \sigma_\theta, \sigma_\theta) = h$, that is, using the homogeneity and pressure independence of g, at each particle there holds [5] $\sigma_\theta - \sigma_r = h/g(-1,0,0) =: h_g$. Then with formula (13), the overall dissipation reads

$$\Pi(D_m \boldsymbol{I}) = \frac{1}{|\Omega|}\int_\Omega \boldsymbol{\sigma} \cdot \boldsymbol{d}\, dx = \frac{1}{|\Omega|}\int_\Omega (\sigma_r d_r + 2\sigma_\theta d_\theta) dx$$

With $\sigma_\theta = \sigma_r + h_g$ and $\mathrm{tr}(\boldsymbol{d}) = 0$ this reduces easily to

$$\Pi(D_m \boldsymbol{I}) = 2h_g D_m \ln(1/f) \tag{23}$$

At this point we could repeat the argument unfolded in the deviatoric case to deduce the maximal interval on the axis of hydrostatic macro-stresses that is contained within the rigidity domain. However, in the context of the representation in eq.(16) we may alternatively deduce, based on the macroscopic flow rule and the homogeneity of $\mathcal{G}$:

$$\boldsymbol{\Sigma} \cdot \boldsymbol{D} = \dot{\Lambda}\boldsymbol{\Sigma} \cdot \frac{\partial \mathcal{G}}{\partial \boldsymbol{\Sigma}} = \dot{\Lambda}\mathcal{H} \Longrightarrow \dot{\Lambda} = \Pi(\boldsymbol{D})/H \tag{24}$$

[4] Eq.(20) remains valid also in the case when the matrix is hardenable, if one defines the macro-measure of hardening by $H := (1/|\Omega|)\int_{\Omega\setminus\omega} h\, dx$.

[5] It is tacitly assumed that $\sigma_\theta \geq \sigma_r$, inequality satisfied if $D_m > 0$, in the tensile case; the argument repeats unchanged when $D_m < 0$, in compression.

In general, the functional dependence of $\mathcal{G}$ on the stress state may be expressed in the form $\mathcal{G}(\boldsymbol{\Sigma}) = \widehat{G}(\boldsymbol{\Sigma'}, \Sigma_m)$ and hence

$$\frac{\partial \mathcal{G}}{\partial \boldsymbol{\Sigma}} = \mathrm{Dev}\left(\frac{\partial \widehat{G}}{\partial \boldsymbol{\Sigma'}}\right) + \frac{1}{3}\frac{\partial \widehat{G}}{\partial \Sigma_m}\boldsymbol{I}$$

For spherical symmetry and isotropy, $\boldsymbol{D} = D_m\boldsymbol{I}$ and $\boldsymbol{\Sigma} = \Sigma_m\boldsymbol{I}$; also due to isotropy, the point $\boldsymbol{\Sigma} = \Sigma_m\boldsymbol{I}$ is a vertex of the macro yield surface and assuming $\mathcal{G}$ is differentiable this implies that $\partial\widehat{G}/\partial\boldsymbol{\Sigma'}(\boldsymbol{0}, \Sigma_m) = \boldsymbol{0}$. The overall flow rule together with eqs.(24) and (23) result in

$$D_m = \frac{\dot{\Lambda}}{3}\frac{\partial \widehat{G}}{\partial \Sigma_m}(\boldsymbol{0}, \Sigma_m) \Longrightarrow \frac{\partial \widehat{G}}{\partial \Sigma_m}(\boldsymbol{0}, \Sigma_m) = \frac{3g(-1,0,0)}{2\ln(1/f)}$$

where, recall, the macro-measure of hardening has been defined by $\mathcal{H} := h$. Integrating between $\Sigma_m^0 = 0$ and the current Σ_m, and taking into account that necessarily $\widehat{G}(\boldsymbol{0}, 0) = 0$, obtains[6]

$$\mathcal{G}(\Sigma_m\boldsymbol{I}, f) = \frac{3g(-1,0,0)}{2\ln(1/f)}\Sigma_m \tag{25}$$

Then, as a preliminary result, we may conclude that the upper bound $\mathcal{F}$, as predicted by the velocity field (18), satisfies to eqs.(22) and (25), its restrictions to the subspaces of deviatoric and spherical tensors being thus known a priori, for any measure g of equivalent stress in the matrix of the RVE.

The main task ahead is to complete the description of $\mathcal{F}$ for general stress states, when neither $\boldsymbol{\Sigma'}$ or Σ_m vanish. Exact formulas, generally valid, can no longer be established. But, in connection with point (**ii**) above, a general methodology of approximating the overall yield function is equally useful. Here we seek an approximation $\mathcal{G}_{apx}$ to the function $\mathcal{G}$, resulting from the velocity field (18), with the following properties: **1)** is convex and positive first degree homogeneous; **2)** it reduces to (22) and (25) on the subspaces of deviatoric and hydrostatic stresses, respectively; **3)** for reasons of symmetry, it has $\boldsymbol{\Sigma} = \Sigma_m\boldsymbol{I}$ as vertex and is symmetric about the hyperplane $\Sigma_m = 0$; **4)** finally, for a set $\{\boldsymbol{D}^{(i)} \,|\, i = 1, ..., n_{data}\}$ such that $\boldsymbol{D'}^{(i)} \neq \boldsymbol{0}$ and $D_m^{(i)} \neq 0$, the corresponding set of macro-stresses $\boldsymbol{\Sigma}^{(i)}$ is calculated by using eqs.(13) and (15), using numerical integration, and then the parameters of $\mathcal{G}_{apx}$ solve the optimization problem

$$\mathrm{Min}\sum_{i=1}^{n_{data}} |\mathcal{G}_{apx}(\boldsymbol{\Sigma}^{(i)}/H) - 1| \tag{26}$$

Within the present theoretical framework, the best "quadratic" approximation is[7]

$$\mathcal{G}_{apx}(\boldsymbol{\Sigma}, f) := \left\{\frac{g^2(\boldsymbol{\Sigma})}{(1-f)^2} + \left[\frac{3/2}{\ln(1/f)}\right]^2 \Sigma_m^2\right\}^{1/2} \tag{27}$$

It satisfies all the requirements listed above except the last, due to an insufficient number of parameters. Because of this it suffers from the same deficiency in the intermediary triaxiliaty range, as mentioned in connection with the formula in eq.(3). However, it may be noticed that this approximation is valid for any yielding criterion g describing matrix response. To improve the accuracy of the description of yielding states with intermediary triaxiality ratios one must consider homogeneous approximations of higher order. This investigation will be unfolded next for the case when the matrix response is described by the Hershey-Hosford function.

3. Overall yield function of a hollow sphere with a Hershey-Hosford matrix

In this section we first develop general formulas for estimating the local dissipation function and its gradient. Then, given the local rate of deformation field (19), the corresponding overall yield surface, when $n = 2$ and $n = 8$ in eq.(2), is first investigated numerically, and then analytical representations are identified.

3.1 General approach

Further progress requires the calculation of the local dissipation function $\pi(\boldsymbol{d})$. In theory, one could use eq.(7), where the plastic multiplier $\dot{\lambda}$ is represented as a function of $\boldsymbol{d}$ by solving the system in eqs.(5-6). However, except for few particular cases (e.g., Mises), this system cannot be solved analytically. Since we aim at a general methodology, we shall adopt a different approach, applicable to any isotropic yield function, and which results in simple estimates of the π-function, with whatever degree of accuracy one may desire.

The principal values of $\boldsymbol{d}$, denoted d_i, $i = 1, 2, 3$, are the solutions of the characteristic equation[8] in μ

$$\det(\boldsymbol{d} - \mu\boldsymbol{I}) = 0 \iff \mu^3 - J_2\mu - J_3 = 0 \tag{28}$$

[6]The same formula describes the overall response in compression, if one substitutes $g(-1,0,0)$ with $g(1,0,0)$ and Σ_m with $-\Sigma_m$.
[7]Assuming tension/compression symmetry, $g(-1,0,0) = g(1,0,0) = 1$, after normalization.
[8]Taking into account that $J_1 := \mathrm{tr}(\boldsymbol{d}) = 0$.

where $J_2(\boldsymbol{d}) := (1/2)|\boldsymbol{d}|^2$, $J_3(\boldsymbol{d}) := \det(\boldsymbol{d})$. By the substitution $\mu = 2\sqrt{J_2/3}\,\widehat{\mu}$, eq.(28) transforms into an equation for the octahedric angle ψ

$$\cos(3\psi) = \frac{3\sqrt{6}J_3}{|\boldsymbol{d}|^3} \tag{29}$$

Letting ψ_d denote its only solution in $[0, \pi/3)$, the principal values of $\boldsymbol{d} = \boldsymbol{d'}$ admit the representation

$$\begin{array}{l} d_1 = d'_1 = \sqrt{2/3}\ |\boldsymbol{d}|\ \cos\psi_d \\ d_2 = d'_2 = \sqrt{2/3}\ |\boldsymbol{d}|\ \cos(\psi_d + 4\pi/3) \\ d_3 = d'_3 = \sqrt{2/3}\ |\boldsymbol{d}|\ \cos(\psi_d + 2\pi/3) \end{array} \tag{30}$$

From eq.(10) we deduce

$$\pi(\boldsymbol{d}) = h \max_{g(\boldsymbol{\sigma}/h) = 1} (\boldsymbol{\sigma}/h) \cdot \boldsymbol{d} \tag{31}$$

The matrix being isotropic, $\boldsymbol{\sigma}$ and $\boldsymbol{d}$ share the same principal axes and hence $\boldsymbol{\sigma} \cdot \boldsymbol{d} = \sigma_i d_i$, where σ_i are the principal values of $\boldsymbol{\sigma}$. Representing σ_i as in eq.(30), with ψ_s denoting the corresponding (octahedric) angle, and using the homogeneity of g, we have

$$g(\boldsymbol{\sigma}/h) = 1 \iff |\boldsymbol{\sigma}|/h = \sqrt{3/2}/\widehat{g}(\psi_s)$$

where

$$\widehat{g}(\psi_s) := g(\cos\psi_s, \cos(\psi_s + 4\pi/3), \cos(\psi_s + 2\pi/3)) \tag{32}$$

Next, due to the isotropy and the tension/compression symmetry of g, it suffices to consider in eq.(31) only a segment of the curve $g(\boldsymbol{\sigma}/h) = 1$ spanning an angle of $\pi/6$ radians; then, using once more eq.(30) for d_i, we obtain

$$\pi(\boldsymbol{d}) = h\sqrt{2/3}\,|\boldsymbol{d}|\,\widehat{\pi}(\psi_d) \tag{33}$$

where

$$\widehat{\pi}(\psi_d) := \max_{\psi_s \in [0, \pi/6]} \eta(\psi_s, \psi_d) \tag{34}$$

$$\eta(\psi_s, \psi_d) := \frac{1}{\widehat{g}(\psi_s)} \sum_{k=0}^{2} \cos(\psi_s + 2k\pi/3)\cos(\psi_d + 2k\pi/3) \tag{35}$$

In the particular case of a von Mises matrix, when $p = 2$ in eq.(2), it can be easily verified that $\widehat{\pi} \equiv 1$, eq.(33) reducing to the well-known formula

$$\pi(\boldsymbol{d}) = h\sqrt{2/3}\,|\boldsymbol{d}| \tag{36}$$

In the general case, of an arbitrary function g, the function $\widehat{\pi}$ can be easily described numerically, by using eqs.(34), (35) and (32) to collect a set of "sampling" points $\{(\psi_d^{(k)}, \widehat{\pi}(\psi_d^{(k)})) \,|\, k = 1, ..., N_\psi\}$, with N_ψ representing the total number of sampling locations $\psi_d^{(k)}$. Then, similarly to Soare and Benzerga (2015), a simple analytic representation of this data set is constructed by calculating its corresponding Fourier series, an obvious choice due to periodicity and symmetry, and thus by approximating

$$\widehat{\pi}(\psi_d) = a_0/2 + \sum_{k \geq 1} a_k \cos(6k\psi_d) \tag{37}$$

where

$$a_k = \frac{12}{\pi} \int_0^{\pi/6} \widehat{\pi}(\psi_d)\cos(6k\psi_d)\, d\psi_d \tag{38}$$

The first 24 coefficients corresponding to the HH-function with exponent $n = 8$ are listed in Table 1. They provide an approximation of $\widehat{\pi}$ with a maximum absolute error less than 10^{-5}, and to its derivative $d\widehat{\pi}/d\psi_d$ with a maximum absolute error less than 10^{-3}.

Considering next the macro stress $\boldsymbol{\Sigma}$, combining eqs.(12,13) and (15), this is calculated with the formula

$$\boldsymbol{\Sigma} = \frac{1}{|\Omega|} \int_{\Omega \setminus \omega} \frac{\partial \pi}{\partial \boldsymbol{D}}\, dx \tag{39}$$

Table 1: Fourier coefficients of $\widehat{\pi}$, eqs.(33), (37-38), when $n = 8$ in the HH function, eq.(2).

a_1	1.95458550	a_5	-0.00068686	a_9	-0.00008491	a_{13}	-0.00002102	a_{17}	-0.00000693	a_{21}	-0.00000267
a_2	0.02611413	a_6	0.00036131	a_{10}	0.00005756	a_{14}	0.00001561	a_{18}	0.00000540	a_{22}	0.00000214
a_3	-0.00447456	a_7	-0.00020961	a_{11}	-0.00004020	a_{15}	-0.00001177	a_{19}	-0.00000424	a_{23}	-0.00000173
a_4	0.00152358	a_8	0.00013013	a_{12}	0.00002878	a_{16}	0.00000898	a_{20}	0.00000336	a_{24}	0.00000140

Given the symmetry of the RVE, the volume integral in eq.(39) can be conveniently expressed in spherical coordinates to obtain, after the substitution $\rho := r^3/b^3$,

$$\boldsymbol{\Sigma} = \frac{1}{4\pi}\int_f^1\int_0^\pi\int_0^{2\pi} \frac{\partial \pi}{\partial \boldsymbol{D}}(\boldsymbol{d}(\rho \boldsymbol{e}_r))\sin\phi\, d\theta\, d\phi\, d\rho \tag{40}$$

here the same symbol, π, denoting both the dissipation and the famous number.

In this investigation, the local rate of deformation field is approximated by eq.(19), which, for numerical purposes, is rewritten as

$$\boldsymbol{d} = \frac{\widehat{\boldsymbol{d}}}{\rho}, \quad \text{with} \quad \widehat{\boldsymbol{d}} := \rho\, \boldsymbol{D'} + D_m\,(\boldsymbol{I} - 3\boldsymbol{e}_r \otimes \boldsymbol{e}_r) \tag{41}$$

By homogeneity, there holds

$$\pi(\boldsymbol{d}) = \pi(\widehat{\boldsymbol{d}})/\rho$$

and then the derivatives involved in eq.(40) are calculated by

$$\frac{\partial \pi}{\partial D_{ij}} = \frac{1}{\rho}\,\frac{\partial \pi}{\partial d_{ab}}(\widehat{\boldsymbol{d}})\,\frac{\partial \widehat{d}_{ab}}{\partial D_{ij}} \tag{42}$$

For the field in eq.(41) we have the formula

$$\frac{\partial \widehat{d}_{ab}}{\partial D_{ij}} = \rho\,(\delta_{ai}\delta_{bj} - \delta_{ij}\delta_{ab}/3) + \frac{\delta_{ij}}{3}\,[\delta_{ab} - 3(\boldsymbol{e}_r \otimes \boldsymbol{e}_r)_{ab}]$$

which substituted into eq.(42) results in

$$\frac{\partial \pi}{\partial D_{ij}} = \frac{\partial \pi}{\partial d_{ij}} - \frac{\delta_{ij}}{3}\frac{\partial \pi}{\partial d_{aa}} + \frac{\delta_{ij}}{\rho}\left[\frac{1}{3}\frac{\partial \pi}{\partial d_{aa}} - \frac{\partial \pi}{\partial d_{ab}}(\boldsymbol{e}_r \otimes \boldsymbol{e}_r)_{ab}\right] \tag{43}$$

Then, with eq.(33), the gradient of the local dissipation reads

$$\frac{\partial \pi}{\partial d_{ab}}(\widehat{\boldsymbol{d}}) = h\sqrt{\frac{2}{3}}\left(\frac{\widehat{d}_{ab}}{|\widehat{\boldsymbol{d}}|}\,\widehat{\pi} + |\widehat{\boldsymbol{d}}|\frac{\partial \widehat{\pi}}{\partial d_{ab}}\right) \tag{44}$$

where $\widehat{\pi}$ is evaluated using eq.(37), its derivatives with respect to d_{ab} by

$$\frac{\partial \widehat{\pi}}{\partial d_{ab}} = \frac{d\widehat{\pi}}{d\psi_d}\,\frac{\partial \psi_d}{\partial d_{ab}} \tag{45}$$

and

$$|\widehat{\boldsymbol{d}}| = \left(\rho^2|\boldsymbol{D'}|^2 - 6\rho D_m \boldsymbol{D'}\cdot \boldsymbol{e}\otimes\boldsymbol{e}_r + 6D_m^2\right)^{1/2}$$

By differentiating in eq.(29) with respect to d_{ab} we get

$$\sin(3\psi_d)\frac{\partial \psi_d}{\partial d_{ab}} = \frac{-\sqrt{6}}{|\widehat{\boldsymbol{d}}|^3}\left(\frac{\partial J_3}{\partial d_{ab}}(\widehat{\boldsymbol{d}}) - \frac{3J_3\widehat{d}_{ab}}{|\widehat{\boldsymbol{d}}|^2}\right)$$

which after substitution in eq.(45) obtains

$$\frac{\partial \widehat{\pi}}{\partial d_{ab}} = \frac{d\widehat{\pi}}{d\psi_d}\,\frac{\sqrt{6}}{|\widehat{\boldsymbol{d}}|^3\sin(3\psi_d)}\left(\frac{3J_3\widehat{d}_{ab}}{|\widehat{\boldsymbol{d}}|^2} - \frac{\partial J_3}{\partial d_{ab}}(\widehat{\boldsymbol{d}})\right) \tag{46}$$

where

$$\frac{d\widehat{\pi}}{d\psi_d} = -6\sum_{k\geq 1} k a_k \sin(6k\psi_d)$$

and

$$\frac{\partial J_3}{\partial d_{11}} = d_{22}d_{33} - d_{23}^2, \quad \frac{\partial J_3}{\partial d_{22}} = d_{11}d_{33} - d_{13}^2, \quad \frac{\partial J_3}{\partial d_{33}} = d_{11}d_{22} - d_{12}^2$$

$$\frac{\partial J_3}{\partial d_{12}} = d_{13}d_{23} - d_{12}d_{33}, \quad \frac{\partial J_3}{\partial d_{13}} = d_{12}d_{23} - d_{13}d_{22}, \quad \frac{\partial J_3}{\partial d_{23}} = d_{12}d_{13} - d_{11}d_{33}.$$

With ψ_d varying within the interval $[0, \pi/6]$, for symmetry reasons, let us note that formula (46) is valid only when $\psi_d \neq 0$. But due to the same symmetry reasons, and because of the assumed smoothness of the dissipation π, it is clear that there must hold

$$\frac{d\widehat{\pi}}{d\psi_d}(\psi_d = 0) = 0 \tag{47}$$

We also observe that, because g is pressure independent, homogeneous, convex and smooth, there holds

$$\widehat{\pi}(\psi_d = 0) = 1 \tag{48}$$

Indeed, from eqs.(34), (35), and (32) we have

$$\widehat{\pi}(0) = \max_{\psi_s \in [0,\pi/6]} \frac{(3/2)\cos\psi_s}{g(s_1, s_2, s_3)}$$

where $s_1 := \cos\psi_s$, $s_2 := -(1/2)\cos\psi_s + (\sqrt{3}/2)\sin\psi_s$ and $s_3 := -(1/2)\cos\psi_s - (\sqrt{3}/2)\sin\psi_s$; by pressure-independence, adding $(1/2)\cos\psi_s$ to all s_i the value of g does not change, and hence $g(s_1, s_2, s_3) = (3/2)\cos\psi_s\, g(1, t, -t)$, where $t := \tan\psi_s\sqrt{3}$; with $g(1, 0, 0) = 1$, our assertion is proved if we show that the function $y(t) := g(1, t, -t)$ is increasing for $t \geq 0$; this follows from the convexity of g: $y''(t) = \partial^2 g/\partial\sigma_2^2 - 2\partial^2 g/\partial\sigma_2\partial\sigma_3 + \partial^2 g\partial\sigma_3^2 \geq 0$, because $(\sigma_2, \sigma_3) \longrightarrow g(1, \sigma_2, \sigma_3)$ is convex; then y' is increasing, and $y'(0) = (\partial g/\partial\sigma_2 - \partial g/\partial\sigma_3)(1, 0, 0) = 0$, and hence $y'(t) \geq 0$.

Combining eqs.(47) and (48) with eqs.(44,45), obtains:

$$\left.\frac{\partial\pi}{\partial d_{ab}}\right|_{\psi_d=0} = h\sqrt{\frac{2}{3}}\,\frac{\widehat{d}_{ab}}{|\widehat{\boldsymbol{d}}|} \tag{49}$$

Having a methodology for calculating the yield stress $\boldsymbol{\Sigma}(\boldsymbol{D})$ corresponding to a direction $\boldsymbol{D}$, we proceed next to the numerical investigation of the macro yield surface. For this, we consider macro-rates of deformation in the form

$$\boldsymbol{D} = (1 - D_m)\boldsymbol{D'} + D_m\boldsymbol{I} \tag{50}$$

where $\boldsymbol{D'} = D'_1\boldsymbol{e}_1 \otimes \boldsymbol{e}_1 + D'_2\boldsymbol{e}_2 \otimes \boldsymbol{e}_2 + D'_3\boldsymbol{e}_3 \otimes \boldsymbol{e}_3$, with

$$\begin{aligned} D'_1 &= \sqrt{2/3}\,\cos\psi_D \\ D'_2 &= \sqrt{2/3}\,\cos(\psi_D + 4\pi/3) \\ D'_3 &= \sqrt{2/3}\,\cos(\psi_D + 2\pi/3) \end{aligned} \tag{51}$$

to construct a discrete set of probing directions in the space of macro-stresses by varying D_m as $D_m^i = (i-1)\Delta D_m$, $i = 1, 2, ..., N_i$, and ψ_D as $\psi_D^j = (j-1)\Delta\psi_D$, $j = 1, 2, ..., N_j$, where $\Delta D_m = 1/(N_i - 1)$ and $\Delta\psi_D = \pi/[6(N_j - 1)]$, with N_i and N_j denoting the numbers of evenly spaced sampling points in the intervals $[0, 1]$ and $[0, \pi/6]$, respectively. $25 \leq N_i \leq 50$ and $50 \leq N_j \leq 100$ provide sufficient detail for porosities $f \leq 0.001$; for lower porosities, because the corresponding stress points are not evenly spaced, additional specific sampling points are required for $0 < D_m < 1$, which can be calculated on a case by case basis. Due to isotropy, holding $D_m = D_m^i$ constant and varying $\psi_D \in \{\psi_D^j\}$ will reveal a plane section $\Sigma_m = const$ through the macro yield surface, which is parallel to the deviatoric $\boldsymbol{\pi}$-plane; holding $\psi_D = \psi_D^j$ constant and varying $D_m \in \{D_m^i\}$ will reveal a plane section $\Sigma_{eq} = const$, which is parallel to the hydrostatic axis. Here Σ_{eq} denotes an appropriate measure of equivalent stress on the subspace of deviatoric tensors. Due to isotropy, once $\Sigma_m = const$ sections are described, their distribution along the hydrostatic axis, that is, the functional correspondence $\Sigma_{eq} = \Sigma_{eq}(\Sigma_m)$, can be identified by investigating only one section $\psi_D = const$; for simplicity and convenience, because usually yield functions are normalized with a uniaxial traction, we shall use the section $\psi_D = \psi_D^1 = 0$.

Finally, after calculating a set of stress points that lie on the macro yield surface, the last step consists in the modeling of this data set, that is, in identifying appropriate analytic functions that best represent the data. Recalling the discussion in the last paragraphs of Section 2, and generalizing the "quadratic" (27), here we shall consider functions of the form

$$\mathcal{F}_{apx}(\boldsymbol{\Sigma}) = \mathcal{G}_{apx}(\Sigma_{eq}, \Sigma_m) - H$$

with

$$\mathcal{G}_{apx}(\Sigma_{eq}, \Sigma_m) := \left[\sum_{k=0}^{N} a_k(f)\Sigma_{eq}^{N-k}\Sigma_m^k\right]^{1/N} \tag{52}$$

where $N \geq 2$ is an even integer. As mentioned in the previous paragraph, Σ_{eq} stands for an appropriate measure of equivalent stress in the subspace of deviatoric tensors. At this point, a discussion regarding the definition of Σ_{eq}, in the general case, is not possible, since only after learning about the particular characteristics of the macro yield surface corresponding to a particular matrix, specific definitions can be made. However, further a priori considerations can be made regarding the representation of the function $\mathcal{G}_{apx}$. The criterion **2)**, at the end of Section 2, is satisfied if we set

$$a_0(f) = \frac{1}{(1-f)^N}, \quad a_N(f) = \left[\frac{3/2}{\ln(1/f)}\right]^N \tag{53}$$

and **3)** if we set $a_k = 0$, for all odd $k \in \{1, 2, 3..., N\}$. Note that this last condition will ensure also the convexity of the function $\mathcal{F}_{apx}$, once the function $\mathcal{G}_{apx}$ is convex. Indeed, $\mathcal{F}_{apx}$ is the composition of $\mathcal{G}_{apx}$ with the convex functions $\boldsymbol{\Sigma} \longrightarrow \Sigma_{eq}$

and $\mathbf{\Sigma} \longrightarrow \Sigma_m$; by symmetry, we may regard $\mathcal{G}_{apx}$ as a function defined in the first quadrant of the plane (Σ_{eq}, Σ_m), where it is isotone[9], because it is positive, homogeneous and convex; these conditions imply the convexity of $\mathcal{F}_{apx}$.

A particular instance of the $\mathcal{G}_{apx}$ function, satisfying satisfying the set conditions and which will be used in what follows, is

$$\mathcal{G}_{apx}(\Sigma_{eq}, \Sigma_m) = \left[\frac{\Sigma_{eq}^N}{(1-f)^N} + S_N + \frac{(3/2)^N \Sigma_m^N}{[\ln(1/f)]^N} \right]^{1/N} \tag{54}$$

with $N = 8$ and

$$S_8 := a_1 \Sigma_{eq}^6 \Sigma_m^2 + a_2 \Sigma_{eq}^4 \Sigma_m^4 + a_3 \Sigma_{eq}^2 \Sigma_m^6 \tag{55}$$

where the coefficients in eq.(52) have been re-indexed for convenience.

The functions $a_k = a_k(f)$ will be identified in a two-step optimization procedure: first, for each value of f in a discrete set $\{f_i\}$ the coefficients $a_k(f_i)$ are optimized to best fit the (Σ_m, Σ_e) data set corresponding to f_i; after collecting the values $\{a_k(f_i)\}$ at a sufficient number of sampling locations $\{f_i\}$, analytic formulas $a_k = a_k(f)$ are sought to best fit the data points $\{f_i, a_k(f_i)\}$.

3.2 Application: $n = 2$, von Mises matrix

With an already vast amount of dedicated literature, this case is instructive here too, primarily because it serves as a test of the numerical implementation of the general theory, and also because the results can be compared against Gurson's estimate of the overall yield function of a hollow sphere with von Mises matrix. It is worth recalling that our objective is a modeling of the macro yield surface as defined by the macro dissipation function Π^+, see the context of eq.(17), while the Gurson function, eq.(1), derives from an overall dissipation Π^{++} which is an upper bound approximation of Π^+, that is $\Pi^+(\boldsymbol{D}) \leq \Pi^{++}(\boldsymbol{D})$, for all $\boldsymbol{D}$.

The model of the macro yield surface adopted here is the function in eq.(54), with $N = 8$ and S_8 defined by eq.(55). The three parameters $a_k(f)$ are identified by the two-step optimization procedure described in the previous subsection. Thus, in the first step, a discrete description of the (Σ_m, Σ_e) plane section corresponding to $\psi_D = 0$ is constructed by calculating numerically (as done in all the numerical descriptions reported here) the integral(s) in eq.(40) for each f in the set

$$\begin{aligned} V_f := \{1/10^4, 5/10^4\} \cup \{j/10^3 \,|\, j = 1, ..., 9\} \cup \{j/10^2 \,|\, j = 1, ..., 9\} \cup \{j/10 \,|\, j = 1, ..., 9\} \\ \cup \{0.2, 0.21, 0.22, 0.23, 0.24, 0.25, 0.3\} \end{aligned} \tag{56}$$

and the corresponding parameters values $a_k(f)$ are identified by solving the optimization problem (26) for each $f \in V_f$.

In the second step, the data sets $\{(f_j, a_k(f_j)) \,|\, f_j \in V_f^2\}$, for $k = 1, 2, 3$, are modeled with appropriate analytic expressions. The functions

$$a_k(f) = \left(a_{k1} f + a_{k2} f^2 + a_{k3} f^3 + a_{k4} f^4\right) / (1-f)^8 \tag{57}$$

with coefficients listed in the first three columns of Table 2, provide a satisfactory representation, as shown in Fig.1, where the first-fit model and Gurson's model are also shown for comparison. Overall, for porosities $f \geq 0.0001$ the resulting model is satisfactory. It may be noticed that, by comparison with the second-fit model, the Gurson model provides a better representation of the $\{(S_{eq}, S_m)\}$ data set for $f \approx 0.0001$, although the first-fit model is the most accurate. This is due the fact that for $f < 0.0001$ the parameters a_k of the model (54-55) do not feature a "natural" variation, monotonic representations as in eq.(57) being less accurate. If needed, the modeling may be extended to lower porosities either by employing a more complex G_{apx} function as in eq.(54), or by modulating Gurson's function with an appropriate multiplier function.

To complete the description of the yield surface one has to specify the measure of equivalent stress Σ_{eq}. As discussed in the previous subsection, this is achieved by investigating $D_m = const$ plane sections through the yield surface. The discrete description for several values of f was constructed by using numerical integration to calculate the integral(s) in eq.(40). The results are similar for all porosities, differing only by a scaling factor. The $D_m = const$ sections corresponding to $f = 0.01$ are shown in projection on the octahedric plane in Fig.2(Left) (only a $\pi/3$ sector was actually calculated, the rest of the figure being constructed by using symmetries). As expected, based on eq.(22), the contour $D_m = 0$, corresponding to $\Sigma_m = 0$, is a (scaled) circle, hence defining the von-Mises measure of equivalent stress $\Sigma_e = \sqrt{3/2}|\mathbf{\Sigma'}|$. On the other hand, the $D_m > 0$ contours do feature slight deviations from the circular shape. This is barely visible to the naked eye in Fig.2(Left) so, for illustration, a zoom in of the section $D_m = 0.3$ is shown in Fig.2(Right). Thus the macro yield surface predicted by the approximation (18) of the velocity field within the RVE features a dependence on the octahedric angle (of the stress space), or, equivalently, on the Lode parameter. Furthermore, the symmetry of the $D_m > 0$ contours does not reduce to the $\pi/6$-symmetry, and hence the corresponding macro measure(s) Σ_{eq} are not symmetric with respect to the origin of the stress space (tension/compression asymmetry). Here the matter is not pursued further, since the circular shape is a good approximation, having also the advantage of a very simple analytical formula by comparison with the quite complex modeling required by the actual variation of Σ_{eq}. This kind of modeling will be illustrated in the next subsection where the RVE with a non-quadratic matrix is investigated.

[9]For vectors, the partial ordering $x \leq y$ means that componentwise there holds $x_i \leq y_i$. A real function $f(x)$ is isotone if $x \leq y \Rightarrow f(x) \leq f(y)$. If $g_i(x)$ are convex real functions such that the set $\{z_i = g_i(x)\}$ is convex, and if the function $f(z)$ is isotone, then the composition $f(g(x))$ is convex, e.g. Borwein and Lewis (2000).

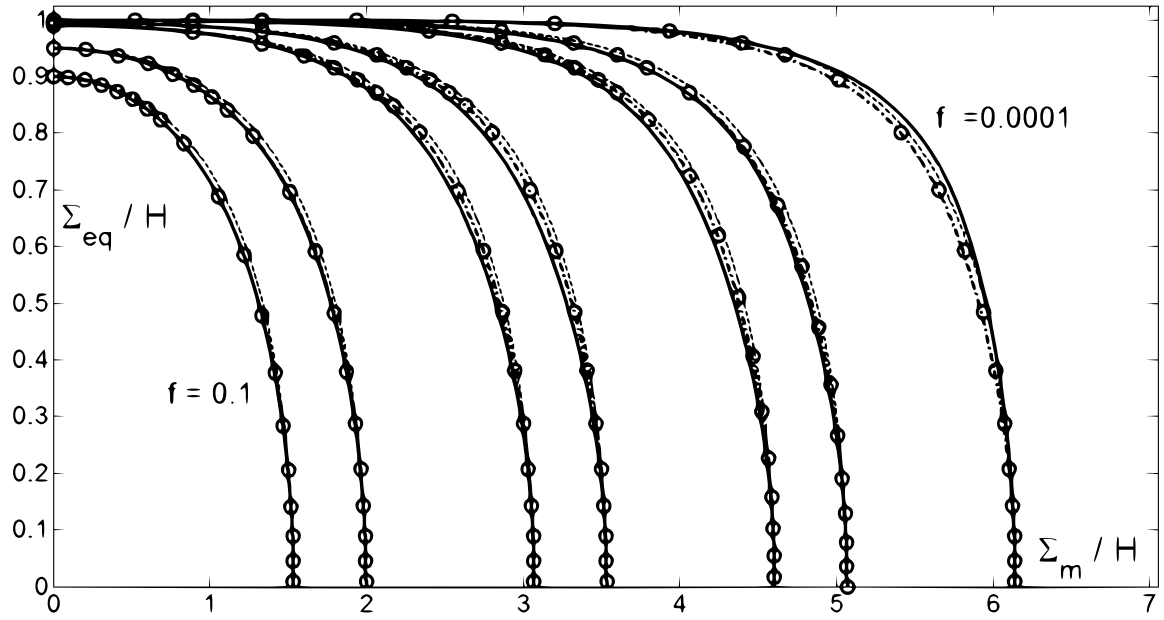

Figure 1: The case $n = 2$. Illustration of the numerical description (small circles) of the (Σ_{eq}, Σ_m) section through the macro yield surface of the rigid hollow sphere, corresponding to $\psi_D = 0$ and porosities $f \in \{0.0001, 0.0005, 0.001, 0.005, 0.01, 0.05, 0.1\}$. Corresponding analytical models, first-fit and second-fit, are shown with line-dot and solid line, respectively. Comparison with Gurson's model (dashed line).

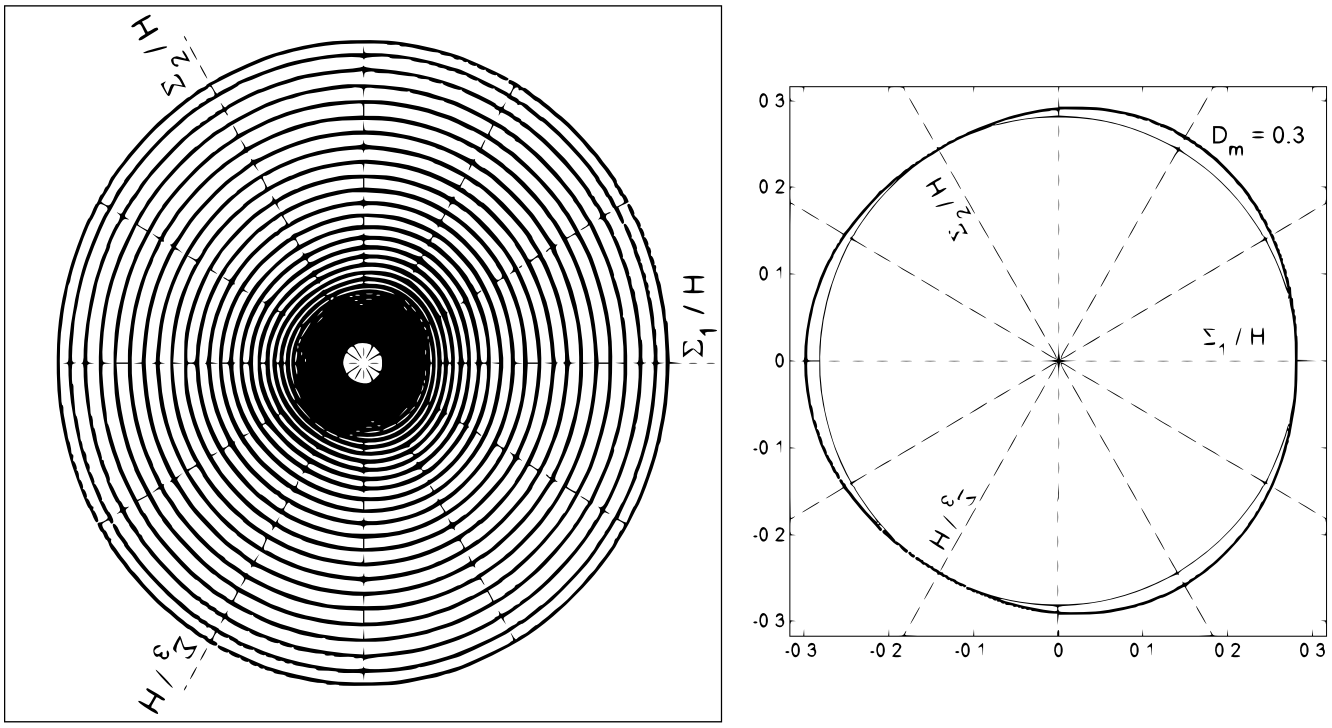

Figure 2: **Left.** $D_m = K$ sections through the numerically calculated macro yield surface, for $n = 2$ and $f = 0.01$; showing increments of $\Delta K = 0.02$, starting from $K = 0.0$ (the outer contour) and up to $K = 0.8$ (the innermost contour). **Right.** Zoom in of the $D_m = 0.3$ section (outer thick line); also shown is a comparison circle drawn in thin line.

3.3 Application: $n = 8$, a non-quadratic matrix

For $n > 2$ the HH-function describes a "softer" material and hence the overall yield surface of the hollow sphere with matrix characterized by $n > 2$ is enclosed by the overall yield surface of the same hollow sphere but with von Mises matrix. Thus the model (54,55) should be applicable also when $n > 2$ and $f \geq 0.0001$. Indeed, the second-fit model in Fig.3, with parameters fitting calculations on the same discrete set of porosities (56) and reported in the last three columns of Table2, shows a good

Table 2: Coefficients a_{kj} of the functions in eq.(57): the first and last three columns correspond to $n = 2$ and $n = 8$, respectively.

a_{11}	9.82087655	a_{21}	2.14157679	a_{31}	0.17407617	a_{11}	12.030132	a_{21}	2.0918194	a_{31}	0.22323416
a_{12}	19.2702540	a_{22}	21.4106372	a_{32}	8.67656750	a_{12}	63.325678	a_{22}	22.285874	a_{32}	14.5105996
a_{13}	-91.2626363	a_{23}	60.2174971	a_{33}	41.3756041	a_{13}	-281.17601	a_{23}	223.09308	a_{33}	52.2364078
a_{14}	135.063309	a_{24}	-74.0578707	a_{34}	-0.86978860	a_{14}	393.96968	a_{24}	-247.70652	a_{34}	16.9516242

agreement with the calculated data, even for $f \approx 0.0001$. The model is less accurate for porosities $f < 0.0001$, for the same reasons described in the previous subsection.

$D_m = const$ sections, corresponding to $\Sigma_m = const$ sections through the macro yield surface, were calculated for several values of f and it was found that they differ only by scaling factors; the ones corresponding to $f = 0.01$ are illustrated Fig.4(Left), in projection on the octahedric plane. The outer $D_m = 0$ contour agrees with formula (22), being precisely the scaled version of the HH-function with $n = 8$ in eq.(2). The most striking feature of the macro yield surface is the gradual change in shape of its $\Sigma_m = const$ sections, from the $\Sigma_m/H = 0$ hexagon with smooth vertices, to triangles, when $\Sigma_m/H \approx 2.9$, and finally to circles, in a vicinity of the limiting value $\Sigma_m/H = (2/3)\ln(1/f) \approx 3.07$, Fig.4(Right). In particular, this also shows a significant tension/compression asymmetry in an intermediary range of triaxialities.

A general approach to the modeling of the corresponding measure Σ_{eq} of equivalent stress in the deviatoric subspace may follow along the lines described in Soare and Benzerga (2015). Here, for the sake of brevity, we shall take advantage of the particularities of the present case and model the variation of Σ_{eq} by the following extended version of the Karafilis and Boyce (1993) function:

$$\Sigma_{eq}(\mathbf{\Sigma'}) = (1-\Lambda)G_A(\mathbf{\Sigma'}) + \Lambda G_B(\mathbf{\Sigma'}) \tag{58}$$

where G_A is the HH-function

$$G_A(\mathbf{\Sigma}) = K_{N_{eq}}\left[|\Sigma_1 - \Sigma_2|^{N_{eq}} + |\Sigma_2 - \Sigma_3|^{N_{eq}} + |\Sigma_3 - \Sigma_1|^{N_{eq}}\right]^{1/N_{eq}} \tag{59}$$

with $K_{N_{eq}} = 2^{(-1/N_{eq})}$, and

$$G_B(\mathbf{\Sigma}) = K_B\left[|\Sigma'_1 - c|\Sigma'_1||^{N_{eq}} + |\Sigma'_2 - c|\Sigma'_2||^{N_{eq}} + |\Sigma'_3 - c|\Sigma'_3||^{N_{eq}} +\right]^{1/N_{eq}} \tag{60}$$

with the normalizing constant K_B (along uniaxial tension) defined by

$$K_B = \frac{1}{3}\left\{[2(1-c)]^{N_{eq}} + 2(1+c)^{N_{eq}}\right\}^{1/N_{eq}} \tag{61}$$

For our modeling purposes it suffices to assume a constant "asymmetry" parameter $c = 0.2$; then the parameters Λ and N_{eq} will be used to model the gradual change in shape of $\Sigma_{eq} = const$ sections, described above, as follows.

Since both G_A and G_B are normalized along uniaxial tension, there holds $\Sigma_{eq}(\tau_t, 0, 0) = \tau_t$, where, in terms of principal stresses, $\Sigma_{eq} = \Sigma_{eq}(\Sigma_1, \Sigma_2, \Sigma_3)$, and $\tau_t > 0$ stands for the magnitude of the yielding uniaxial tensile stress. Then the yielding condition for a uniaxial compressive stress, $\Sigma_{eq}(-\tau_c, 0, 0) = \tau_t$ leads to the following formula expressing the parameter Λ in terms of the tension/compression asymmetry ratio $r_{uax} := \tau_t/\tau_c$ and N_{eq}:

$$\Lambda = \frac{\tau_t - \tau_c}{\tau_c\left[G_B(-1,0,0) - 1\right]} = \frac{r_{uax} - 1}{\left\{\dfrac{[2(1+c)]^{N_{eq}} + 2(1-c)^{N_{eq}}}{[2(1-c)]^{N_{eq}} + 2(1+c)^{N_{eq}}}\right\}^{1/N_{eq}} - 1} \tag{62}$$

The tension/compression asymmetry ratio r_{uax} and the exponent N_{eq} vary along the hydrostatic axis. Their functional dependence [10] $r_{uax} = r_{uax}(\Sigma_m/H)$ and $N_{eq} = N_{eq}(\Sigma_m/H)$ can be inferred from the numerically calculated macro yield surface for one instance of the porosity f: for a section $\Sigma_m/H = const$, the uniaxial stresses in tension and compression correspond to the angles on the octahedric plane $\Psi = 0$ and $\Psi = \pi/3$, respectively; then the exponent N_{eq} corresponding to Σ_m/H is found by optimizing the contour $(1-\Lambda)G_A(\mathbf{\Sigma'}/H) + \Lambda G_B(\mathbf{\Sigma'}/H) = \Sigma_{eq}/H$, here Σ_{eq} representing the unique *numerical* value corresponding to Σ_m via the equation $G_{apx}(\Sigma_{eq}, \Sigma_m) = H$, to best fit the shape of the $\Sigma_m/H = const$ contour.

Fig.5(Right) shows the data points for r_{uax} and N_{eq}, extracted from the numerical description of the macro yield surface corresponding to $f = 0.01$, shown in Fig.4. Functions that model the variations of r_{uax} and N_{eq} are as follows:

$$r_{uax}(S_m/H, f) = \begin{cases} 1, \text{ if } S_m/H \le x_1 \\ \phi(S_m/H, x_1, y_1, x_0, y_0, C_1), \text{ if } x_1 \le S_m/H \le x_0 \\ \phi(S_m/H, x_0, y_0, x_2, y_2, C_2), \text{ if } x_0 \le S_m/H \le x_2 \end{cases} \tag{63}$$

[10] An equally valid parameter is the triaxiality ratio $t := \Sigma_m/\Sigma_{eq}$: if, say, Σ_m/H is given, the *numerical* value Σ_{eq}/H is found by solving the equation $G_{apx}(\Sigma_{eq}/H, \Sigma_m/H) - 1 = 0$, thus determining the uniquely corresponding ratio t and hence defining a one-to-one relationship $t = t(\Sigma_m/H)$ for values $\Sigma_m/H \in [0, (2/3)\ln(1/f))$.

where $x_2 = (2/3)\ln(1/f)$ stands for the maximum value of Σ_m/H, $x_0 = x_2 - \Delta_0$, with $\Delta_0 = 0.0911346$, and $x_1 = x_0 - \Delta_1$, with $\Delta_1 = 0.78$; $y_0 = 0.775$ is the minimum value of r_{uax}, and $y_1 = y_2 = 1.0$ are the values of r_{uax} at $\Sigma_m/H = 0$ and x_2, respectively; $C_1 = 24.0$ and $C_2 = 0.5$;

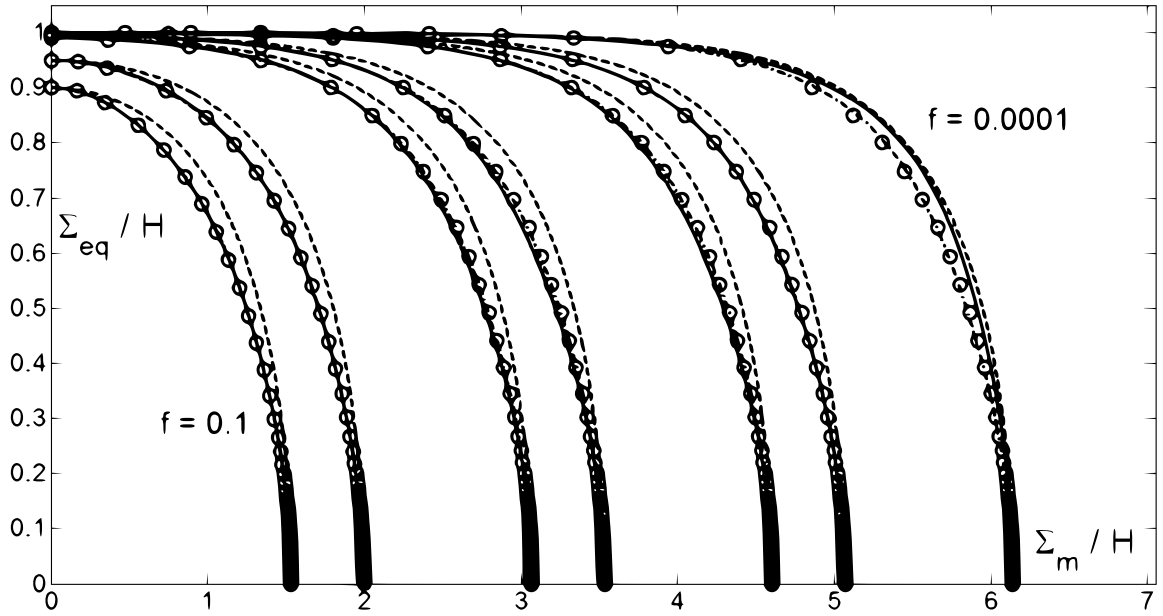

Figure 3: The case $n = 8$. Illustration of the numerical description (small circles) of the (Σ_{eq}, Σ_m) section through the macro yield surface of the rigid hollow sphere, corresponding to $\psi_D = 0$ and porosities $f \in \{0.0001, 0.0005, 0.001, 0.005, 0.01, 0.05, 0.1\}$. Corresponding analytical models, first-fit and second-fit, are shown with line-dot and solid line, respectively. Comparison with Gurson's model (dashed line).

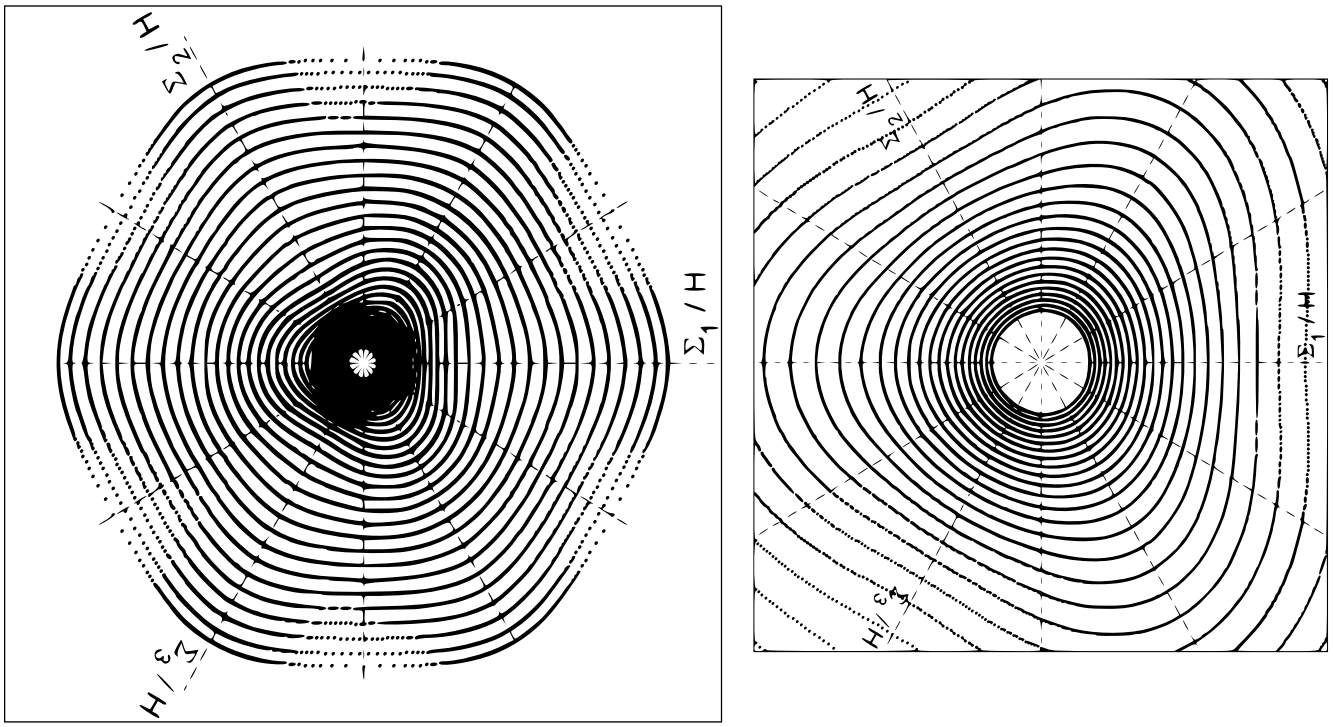

Figure 4: **Left.** $D_m = K$ sections through the numerically calculated macro yield surface, for $n = 8$ and $f = 0.01$; showing increments of $\Delta K = 0.02$, starting from $K = 0.0$ (the outer contour) and up to $K = 0.8$ (the innermost contour). **Right.** Zoom in, showing in greater detail the "inner" (or higher on the pressure axis) $D_m = const$ sections through the macro yield surface.

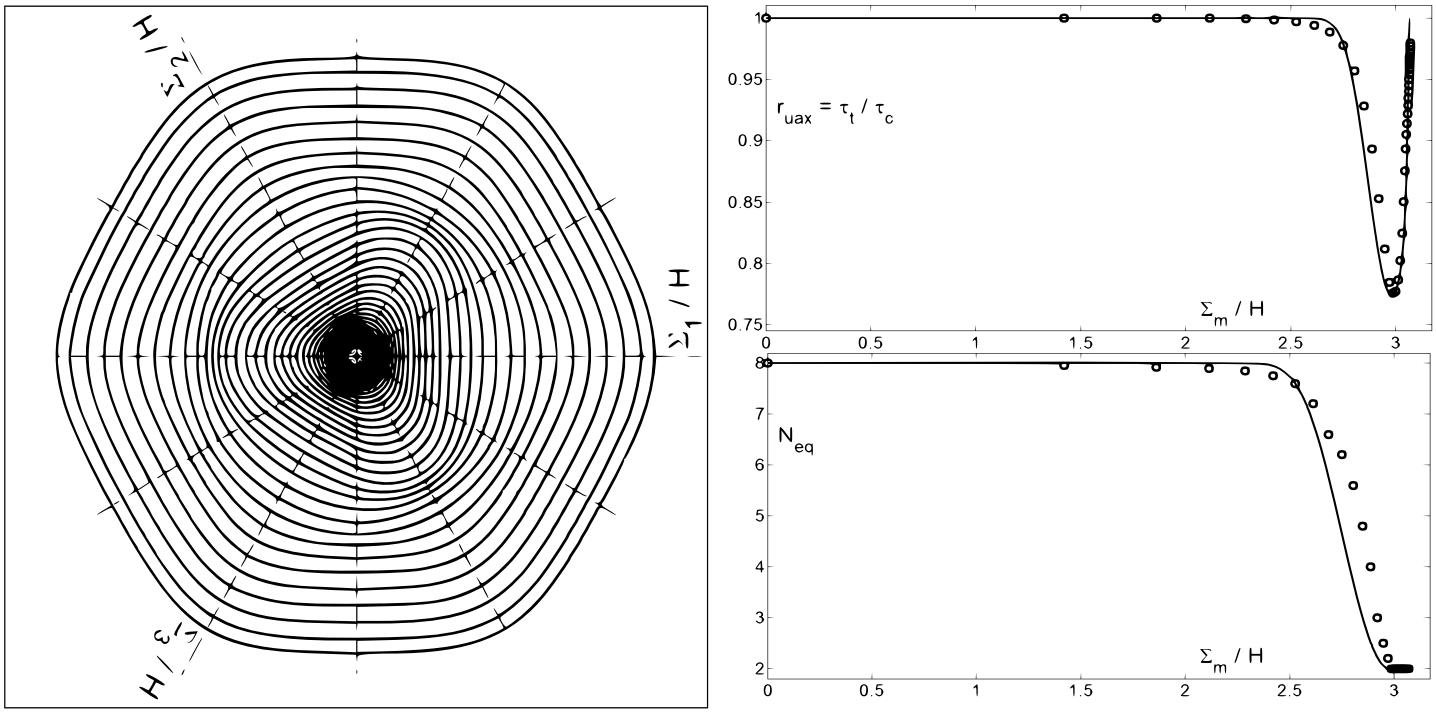

Figure 5: **Left.** Illustration of the model in eqs.(58-65) of the macro yield surface, for $f = 0.01$: $\Sigma_m/H = const$ sections corresponding to the $D_m = const$ sections shown in Fig.4. **Right.** Variations of the parameters r_{uax} and N_{eq} for $f = 0.01$.

$$N_{eq}(S_m/H, f) = \begin{cases} y_1, \text{ if } S_m/H \le x_1 \\ \phi(S_m/H, x_1, y_1, x_0, y_0, C_3), \text{ if } x_1 \le S_m/H \le x_0 \\ y_2, \text{ if } x_0 \le S_m/H \le x_2 \end{cases} \tag{64}$$

where x_0 and x_2 are the same as for r_{uax}, $x_1 = x_0 - \Delta_3$, with $\Delta_3 = 0.98$; here $y_1 = 8$ and $y_2 = 2$ are the values of N_{eq} at $\Sigma_m/H = 0$ and x_2, respectively; $C_3 = 10.0$. The function ϕ is intended to model a rapid, yet smooth transition between two horizontal asymptotes y_1 and y_0, ending and beginning, respectively, at x_1 and x_0; here this is defined by

$$\phi(x, x_1, y_1, x_0, y_0, C) = A + \frac{B}{1 + \exp\left[\dfrac{-C(x_1 - x_0)^2}{(x_1 - x_0)^2 - (x - x_0)^2}\right]} \tag{65}$$

with $A = (y_0 - q y_1)/(1-q)$, $B = (y_1 - y_0)/(1-q)$, $q = 1/(1+\exp(-C))$. Fig.5(Left) shows the contours on the octahedric plane of the macro yield surface, corresponding to $f = 0.01$, as modeled by eqs.(58-65) (together with eqs.(54-55)). Comparison with Fig.4(Left) shows good agreement between model and numerical calculations.

As mentioned before, the macro yield surfaces corresponding to different porosity ratios f share the same "topology", as described for the $f = 0.01$-instance; this is reflected by the fact that r_{uax} and N_{eq} depend on f only through x_2, x_1 and x_0, the rest of their parameters being constants. To illustrate this aspect, in Fig.6 are shown for $f = 0.001$ the numerically calculated macro yield surface (Left) and its model (Right). Then, adopting a geometric perspective, it may be concluded that the overall yield surface of the hollow sphere, as predicted by the velocity field (18), is a cylinder with a top; the wall of the cylinder corresponds to a range where yielding is practically symmetric, while its top features a significant tension/compression asymmetry.

4. Summary

A general methodology for the numerical investigation of the overall yield function of a representative volume element (RVE) of a porous metal has been described and applied here to the modeling of an RVE idealized in the form of a rigid-plastic hollow sphere. The essential inputs are the micro velocity field, compatible with the overall rate of deformation, and the yielding criterion of the matrix, which both may be arbitrary; the essential step consists in the accurate numerical calculation of the micro (local) dissipation field corresponding to a micro-velocity and a yielding criterion.

The approximation of the micro velocity field assumed by Gurson was also used here, mainly because of simplicity, allowing for a priori deductions in the purely deviatoric and hydrostatic cases, but also because a thorough and rigorous investigation of the predictions of this assumption was lacking. Indeed, previous investigations into the problem have followed closely the path set by Gurson's analysis, thereby adopting an upper bound estimation of the corresponding overall dissipation, while here this was calculated numerically, directly from the assumed local velocity field.

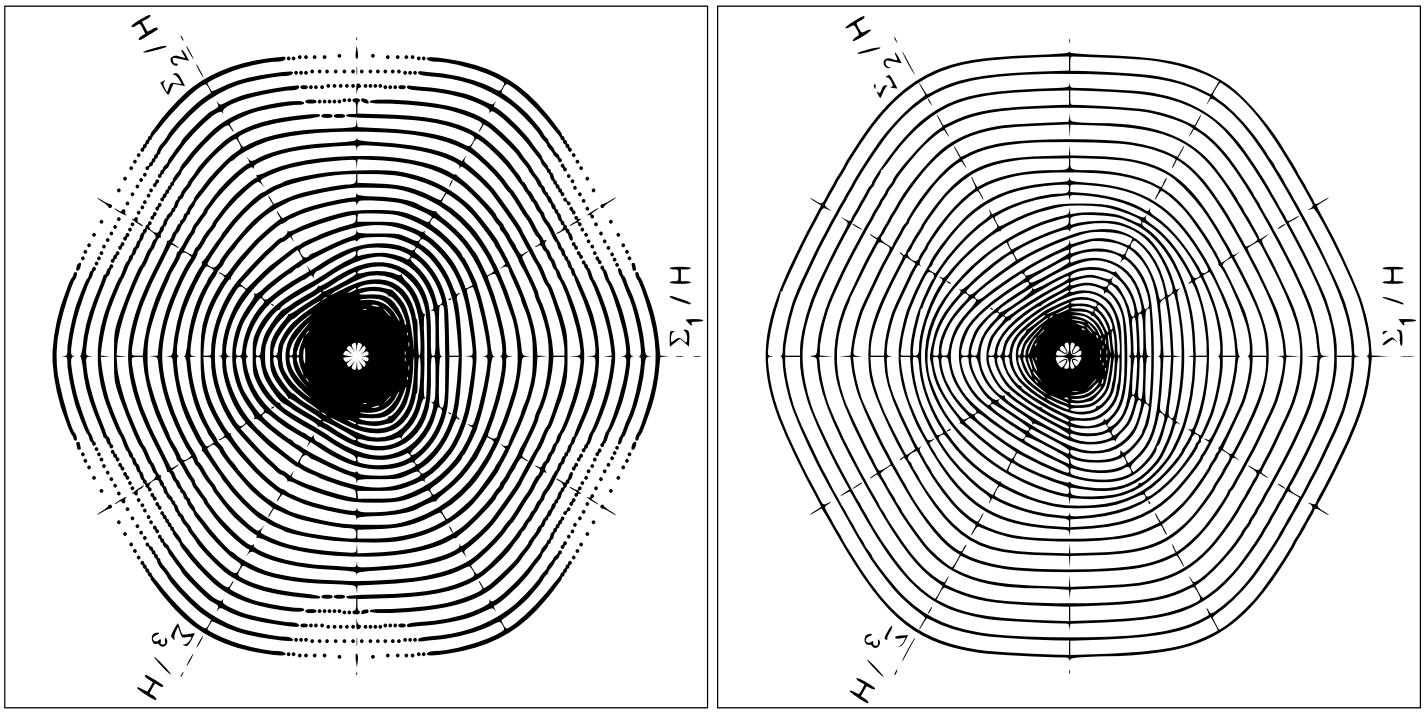

Figure 6: Porosity ratio $f = 0.001$. **Left.** $D_m = const$ sections through the numerically calculated macro yield surface (for $const = 0.0$ with increment of 0.02 up to 0.7). **Right.** The model in eqs.(58-65) of the macro yield surface: $\Sigma_m/H = const$ sections corresponding to the $D_m = const$ sections shown in the left figure.

The calculations for the RVE with von Mises matrix have revealed a dependence of the overall yield function on the octahedric angle (or Lode parameter) and also a certain asymmetry with respect to the origin of the (macro) stress space. However, these deviations from the von Mises norm (equivalent stress) are small and in this case the Gurson function is confirmed to be a good approximation of the overall yield function.

In the case of the RVE with a Hershey-Hosford (exponent $n = 8$) matrix, the predicted overall yield surface has complex features in the range of high triaxialities: significant variations in shape and asymmetry with respect to the origin of the (macro) stress space. An eight order homogeneous polynomial in the (Σ_{eq}, Σ_m)-plane provides a good model for porosity ratios $f \geq 0.0001$. To capture the variation in shape from low to high triaxialities, the equivalent stress Σ_{eq} was modeled by using an extension of the Karafilis and Boyce (1993) function.

Acknowledgement
During the writing of the manuscript the author has benefited from discussions with Amine A. Benzerga. These are gratefully acknowledged.

References

Benzerga, A.A., Besson, J., 2001. Plastic potentials for anisotropic porous solids. Eur. J. Mech. A/Solids, 20, 397-434

Borwein, J.M., Lewis, A.S., 2000. Convex Analysis and Nonlinear Optimization. Springer-Verlag, New York, NY, USA.

Castaneda, P.P., 1991. The effective mechanical properties of nonlinear isotropic composites. J. Mech. Phys. Solids, 39, 45-71.

Cocks, A.C.F., 1989. Inelastic deformation of porous materials. J. Mech. Phys. Solids, 37, 693-715.

Gurson A.L., 1977. Continuum theory of ductile rupture by void nucleation and growth: Part I - Yield criteria and flow rules for porous ductile media. J. Eng. Mat. Tech. 99, 2-15.

Hershey, A.V., 1954. The plasticity of an isotropic aggregate of anisotropic face centred cubic crystals. J. Appl. Mech., 21, 241-249.

Hosford, W.F., 1972. A generalized isotropic yield criterion. J. Applied Mech., 39,607-609.

Karafillis, A.P., Boyce, M.C., 1993. A general anisotropic yield criterion using bounds and a transformation weighting tensor. J. Mech. Phys. Solids, 41, 1859-1886.

Leblond J.B., 2003. La mecanique de rupture fragile et ductile. Hermes Science, Paris. Ch. 7.

Liao, K.C., Pan, J., Tang, S.C., 1997. Approximate yield criteria for anisotropic porous ductile ductile sheet metals. Mech. of Materials, 26, 213-226.

Michel, J.C., Suquet, P., 1992. The constitutive law of nonlinear viscous and porous materials. J. Mech. Phys. Solids, 40, 783-812.

Rice J.R., Tracey D.M., 1969. On the enlargement of voids in triaxial stress fields. J. Mech. Phys. Solids, 17, 201-217.

Soare, S.C., Benzerga, A.A., 2015. On the modeling of asymmetric yield functions. In print at Int. J. Solids and Struct.

Willis, J.R., 1991. On methods for bounding the overall properties of nonlinear composites. J. Mech. Phys. Solids, 39, 73-86.